Article

Not peer-reviewed version

Three-Dimensional Geological Modeling and Hydrothermal Titanite Geochronology of the Antas Norte ISCG Deposit: Implications for the Archean to Paleoproterozoic Fluid Evolution in the Carajás Province

Sergio Roberto Bacelar Huhn *, Rafael Nascimento Paula, Francisco José Fonseca Ferreira, Isac Brito Barreira

Posted Date: 25 August 2025

doi: 10.20944/preprints202508.1721.v1

Keywords: ISCG deposit; Copper; Carajás; geological modeling

 doi:10.20944/preprints202508.1721.v1

Article

Three-Dimensional Geological Modeling and Hydrothermal Titanite Geochronology of the Antas Norte ISCG Deposit: Implications for the Archean to Paleoproterozoic Fluid Evolution in the Carajás Province

Sergio Roberto Bacelar Huhn, Rafael Nascimento Paula, Francisco José Fonseca Ferreira, Isac Brito Barreira

Federal University of Ceará (UFC), Department of Geology, Fortaleza, Brazil; sergio.bacelar@ufc.br

Abstract

The Antas Norte mine, located in the southeastern portion of the Amazonian Craton within the Carajás Mineral Province, is hosted by mafic and felsic metavolcanic rocks that have undergone extensive hydrothermal alteration. Fieldwork and petrographic analyses reveal a hydrothermal sequence comprising sodic (albite), potassic (biotite + scapolite), calcic (amphibole + apatite), silicification (quartz), and propylitic (chlorite + epidote + calcite) assemblages. Mineralization, associated with calcic alteration, occurs in massive, brecciated bodies and vein networks, predominantly composed of chalcopyrite, pyrrhotite, and pyrite. The absence of iron oxides and dominance of iron sulfides classify Antas Norte as an Iron Sulfide Copper-Gold (ISCG) deposit, a subtype of the Iron Oxide Copper-Gold (IOCG) group. The deposit may represent a deeper and more reduced counterpart within the regional IOCG mineralization spectrum, similar to ilmenite-rich Iron Oxide-Apatite (IOA) systems.

Keywords: ISCG deposit; Copper; Carajás; geological modeling

1. Introduction

The Carajás Mineral Province (CMP), located in the southeastern Amazonian Craton, is the Brazil's most significant mineral province and one of the most important globally. It is renowned for its high-grade iron, manganese, platinum group elements (PGE), nickel, and, notably, its Iron Oxide Copper-Gold (IOCG) deposits. Since the discovery of the Salobo and Sossego deposits, Carajás has been a key area for understanding IOCG systems and their diverse geological expressions.

Despite considerable advances, many aspects regarding the diversity of mineralization types within the province remain poorly understood. In particular, the Iron Sulfide Copper-Gold (ISCG) subtype, characterized by abundance of iron sulfides rather than oxides, has been little explored. The Antas Norte deposit presents a rare opportunity to study this less common mineralization expression.

This study integrates fieldwork, petrographic analyses, structural interpretation, and 3D geological modeling to characterize the Antas Norte deposit. By delineating hydrothermal alteration patterns, mineralization styles, and structural controls, the study aims to better understand the processes controlling mineralization in reduced environments within the Carajás Province.

2. Regional Geological Context

The Carajás Mineral Province (CMP) is part of the southeastern Amazonian Craton and comprises Archean basement rocks, Neoarchean supracrustal sequences, and Paleoproterozoic

 doi:10.20944/preprints202508.1721.v1

intrusions. The province is subdivided into two major domains—the Rio Maria and Carajás domains—separated by an east-west trending shear zone (Santos, 2003).

The Carajás Domain hosts the Xingu and Pium Complexes, the Rio Novo Group, and the Itacaiúnas Supergroup, as well as granitoid magmatism events spanning from 2.76 Ga to 1.88 Ga (Hirata et al., 1982; Machado et al., 1991). These geological units present a complex evolutionary history, marked by extensive hydrothermal activity and multiple mineralization events (Figure 1)

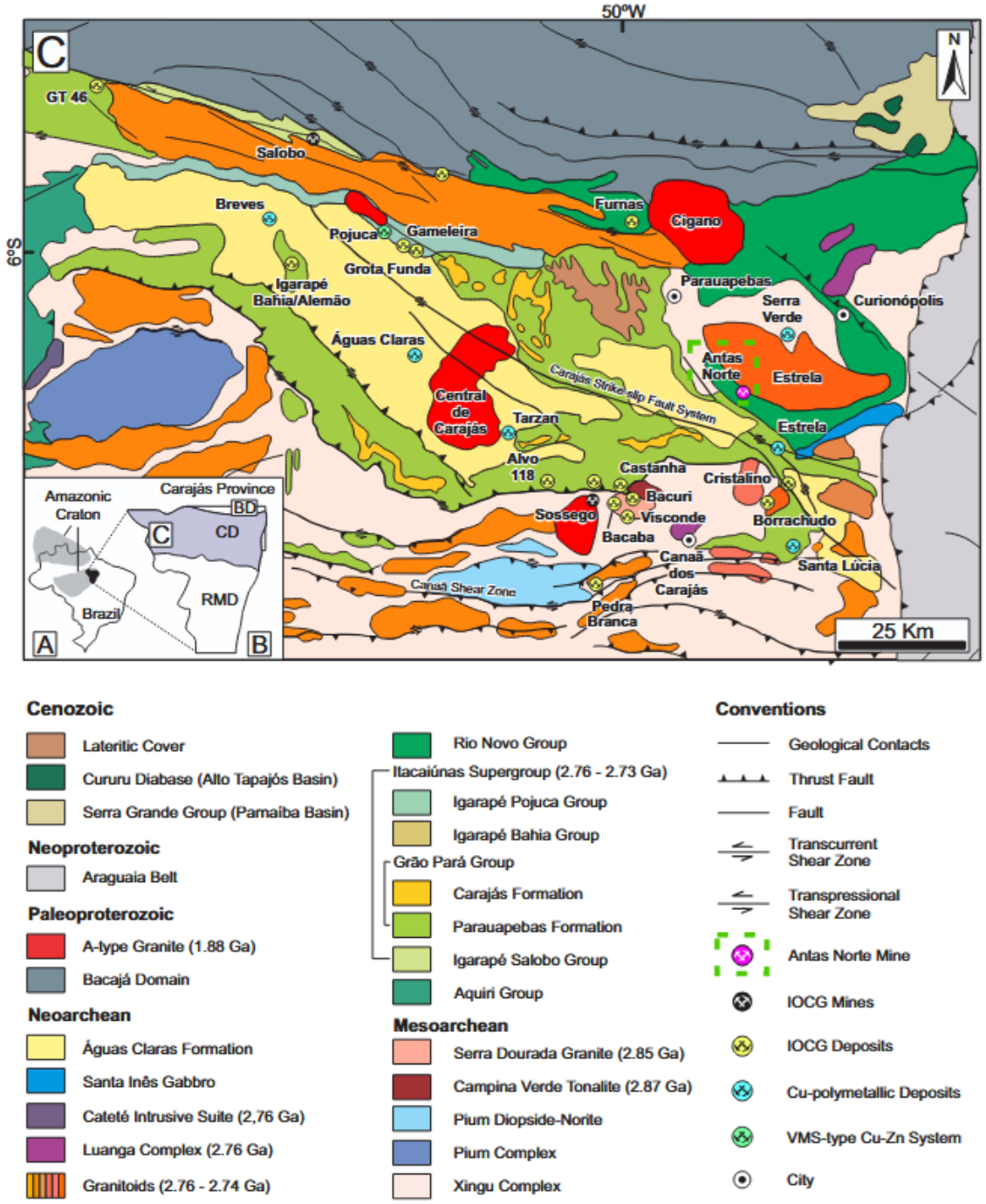

Figure 1. (A) Location of the Carajás Province (black) in the Amazon Craton (light gray). (B) Compartmentalization of the Carajás Province into the Rio Maria domain (south) and the Carajás domain (north). (C) Simplified geological map of the Carajás domain, indicating the location of major copper deposits and structures (Modified from Vasquez et al. 2008).

The Carajás Domain is characterized by the Mesoarchaean base.

 doi:10.20944/preprints202508.1721.v1

3. Iron Oxide Copper-Gold (IOCG) Deposits in the Carajás Province

The IOCG deposit class emerged as a major exploration target following the discovery of the Olympic Dam deposit in Australia (Roberts & Hudson, 1983). IOCG systems typically exhibit significant copper reserves and grades, along with enrichment in elements such as Au, Ag, U, REE, Co, and Ni. However, there are no universally accepted genetic models , given the broad diversity of host rocks, structural settings, alteration styles, and fluid sources (Hitzman, 2000; Williams et al., 2005).

In the Carajás Province, IOCG deposits show a wide range of hydrothermal alterations and ore mineral assemblages, reflecting diverse crustal levels of formation and fluid evolutions (Xavier et al., 2010, 2012).

Key characteristics of Carajás IOCG deposits include:

- Metavolcano-sedimentary host rocks from the Itacaiúnas Supergroup;
- Strong structural control, often associated with shear zones;
- Proximity to diverse intrusive suites (granite, diorite, gabbro);
- Abundant hydrothermal breccias;
- Intense sodic, potassic, and magnetite alterations;
- Polymetallic enrichment (REE, P, U, Ni, W, Sn, Co, Pd);
- Wide variation in formation temperatures (100–570°C) and salinities (0–69 wt.% NaCl eq.).

Deposits in the northern sector (e.g., Salobo, Grota Funda) are associated with the Cinzento Shear Zone and exhibit high-temperature potassic alteration, whereas southern deposits (e.g., Sossego, Cristalino) are controlled by the Canaã Shear Zone and present sodic-calcic to potassic alteration sequences (Monteiro et al., 2008a; Moreto, 2013).

4. Materials and Methods

4.1. Fieldwork, Petrography, and SEM Analyses

Field investigations at the Antas Norte mine included the description of 10 drill cores and 9 outcrops. Observations focused on deposit geometry, lithology, hydrothermal alteration, and mineralization styles.

Petrographic analyses of 34 samples were conducted at the Federal University of Ceará (UFC) to characterize hydrothermal alteration assemblages and ore mineral associations. Additionally, Scanning Electron Microscopy (SEM) combined with Energy Dispersive X-Ray Spectroscopy (EDS) was used to determine the chemical composition of accessory and ore minerals.

4.2. 3D Geological Modeling and Structural Analysis

Three-dimensional modeling was performed using the Leapfrog Geo 2022 software, integrating:

- Geological surface maps,
- Drill hole datasets (totaling 30,657.55 meters),
- Detailed topographic surveys.

Structural measurements (n=57) of faults, fractures, and stretching lineations were analyzed using the Stereonet software to determine the kinematic evolution and structural mineralization controls .

5. Local Geology

5.1. Host Rocks

The Antas Norte deposit is located near the Estrela Granite Complex and is hosted by mafic and felsic metavolcanic rocks belonging to the Grão Pará Group, part of the Itacaiúnas Supergroup (Figure 2). Gabbro dikes crosscut the host sequence and the mineralized zones. Regional structures

 doi:10.20944/preprints202508.1721.v1

have WNW-ESE trend, linked to the Carajás Fault, whereas the ore body is aligned along a NE–SW secondary shear zone.

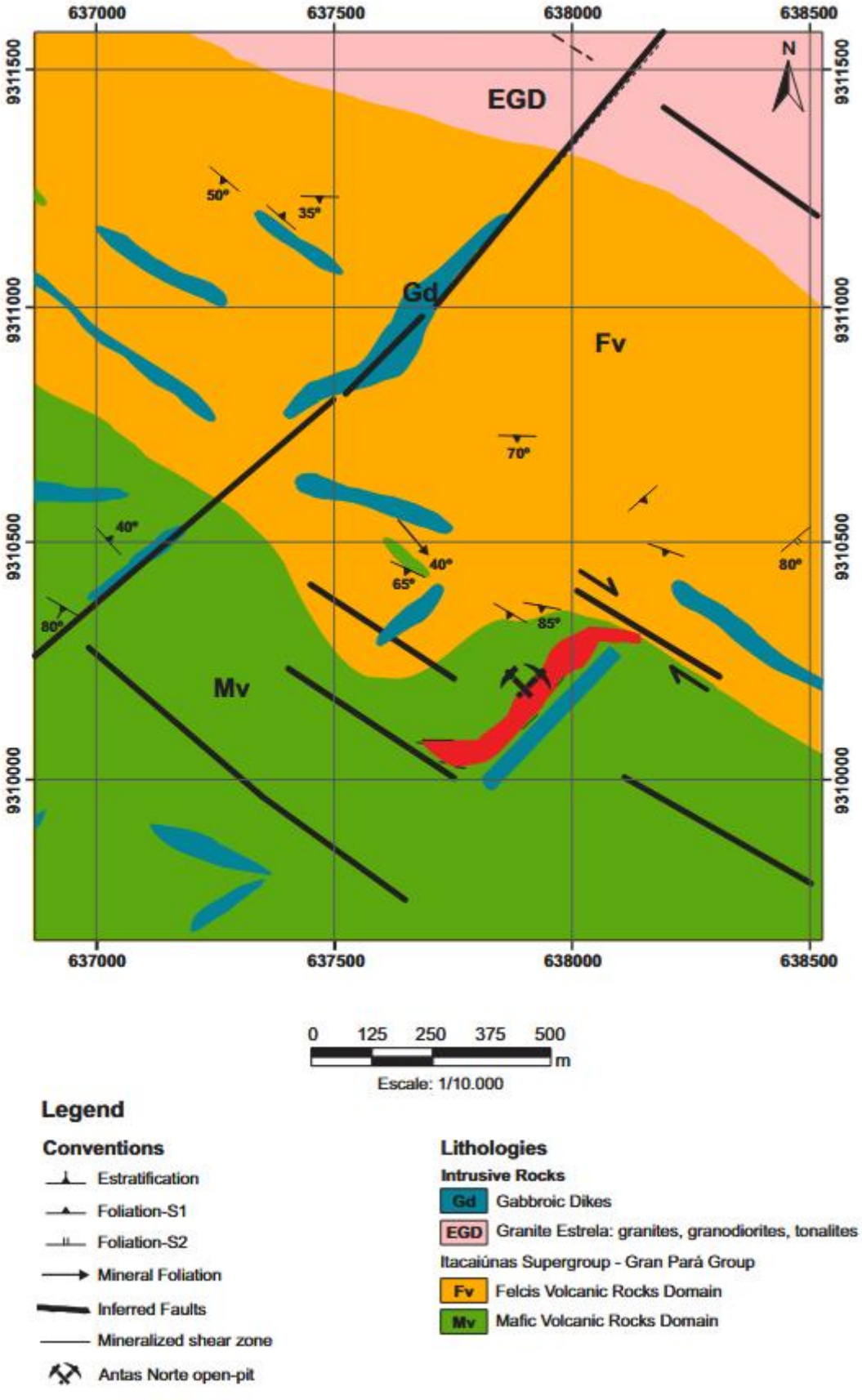

Figure 2. Geological map of the Antas Norte mine area (Modified from Oz Minerals internal files).

 doi:10.20944/preprints202508.1721.v1

Mafic volcanic rocks (Figure 3) exhibit fine to medium grain size and dark gray to greenish color. These rocks present varying shearing degrees and hydrothermal alteration, which have obliterated up to 90% of their original mineralogy. In the distal parts of the deposit, penetrative mylonitic foliation (Figure 3A) is observed, while brecciation (Figure 3B) is common in proximal zones. Despite the extensive alteration, the presence of relic minerals, such as clinopyroxene (Figure 3F), k-feldspar (Figure 3E), and titanite (or ilmenite) (Figure 3D), provides clues about their original composition. Hydrothermal minerals, including amphiboles (hornblende and actinolite) (Figure 3) and biotite (Figure 3F), replaced most primary minerals. Other alteration minerals include apatite (Figure 3B and 3E), scapolite (Figure 3F), chlorite (Figure 3D), ilmenite (Figure 3B and 3D), and epidote (Figure 3E). Albite (Figure 3A and 3C), quartz (Figure 3A and 3C), and chalcopyrite (Figure 3B) are also present, especially near felsic volcanic rocks and mineralization zones.

Primary minerals, such as clinopyroxene, K-feldspar, and titanite (or ilmenite), are preserved as relics within a matrix dominated by hydrothermal minerals, including hornblende, actinolite, biotite, scapolite, chlorite, and apatite. Albite and quartz are present, especially near felsic volcanic rocks and mineralized zones.

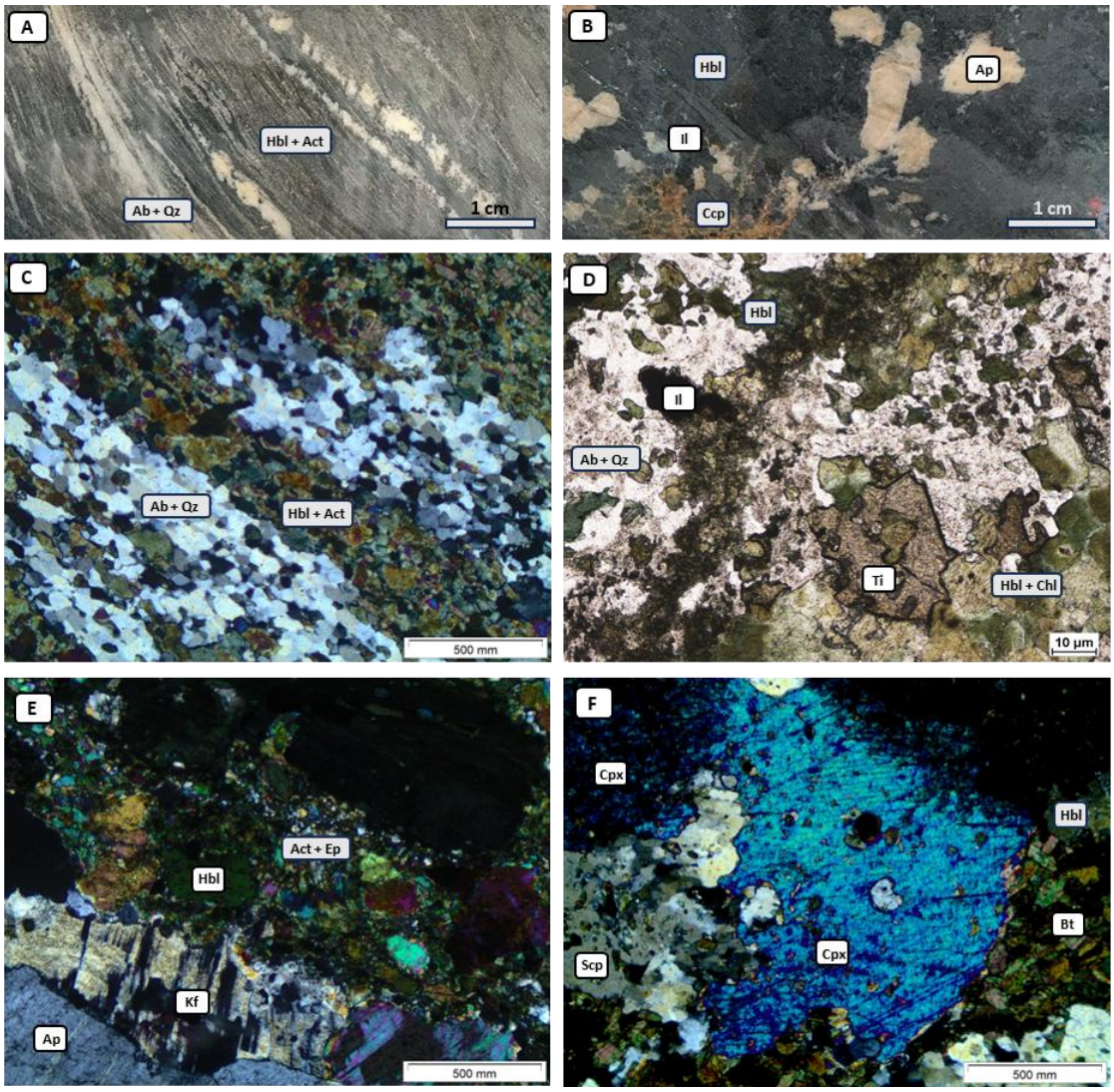

Figure 3. Mafic lithotypes from the Antas Norte mine area: (A) Mafic volcanic rock from the distal mineralization zone, showing mylonitization with hornblende, actinolite, albite, and quartz bands. (B) Brecciated mafic volcanic rock from the proximal mineralization zone, with hornblende, apatite, ilmenite, and chalcopyrite. (C) Photomicrograph (transmitted light—PPL) showing mylonitic banding, with mafic portions (Hbl+Act) and felsic portions (Ab+Qz). (D) Photomicrograph (PPL) of hydrothermally altered rock, showing albite, quartz, hornblende, chlorite, and ilmenite; titanite relics suggest protolithic origin. (E) Photomicrograph (XPL) of the

 doi:10.20944/preprints202508.1721.v1

proximal mineralization, showing significant alteration with apatite, hornblende, actinolite, epidote, and partially consumed k-feldspar. (F) Photomicrograph (XPL) showing intense alteration, with scapolite, biotite, and hornblende, alongside relict clinopyroxene. Abbreviations: Ab: albite; Act: actinolite; Ap: apatite; Bt: biotite; Ccp: chalcopyrite; Chl: chlorite; Cpx: clinopyroxene; Ep: epidote; Scp: scapolite; Hbl: hornblende; Il: ilmenite; Kf: k-feldspar; Qz: quartz; Ttn: titanite; XPL: crossed nicols; PPL: parallel nicols.

5.2. Felsic Volcanic Rocks

Felsic volcanic rocks are fine-grained, presenting light gray to reddish coloration, moderately brecciated, and intensely altered. Phenocrysts of feldspar and quartz occur in a fine-grained albite-quartz matrix, suggesting dacitic composition. Sodic alteration is dominant, characterized by pervasive albite replacement. Hornblende and calcite are common near mafic-felsic contacts.

Felsic volcanic rocks (Figure 4A, 4C, and 4E) are fine-grained with light gray to reddish coloration. Brecciation is moderate, and hydrothermal alteration is prominent, with feldspar (Figure 4E) and quartz phenocrysts (Figure 4C and 4E) set in a fine-grained albite (Figure 4E) and quartz matrix, indicating dacitic composition. Sodium alteration is dominant, forming albite as the main hydrothermal product. Amphiboles (Figure 4A and 4C) and calcite (Figure 4C, 4E and F) are present near contacts with mafic rocks.

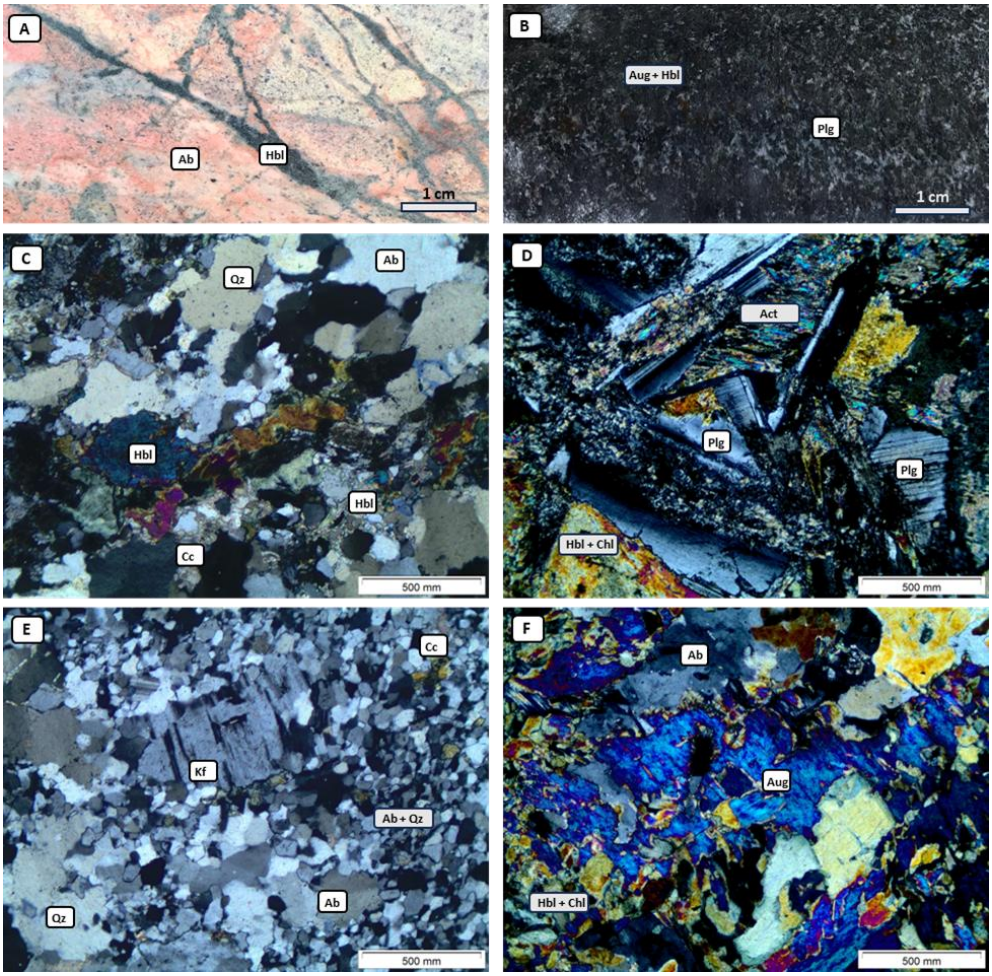

Figure 4. Felsic lithotypes and gabbros from the Antas Norte mine area: (A) Felsic volcanic rock showing brecciation with albite (white/pink) and hornblende veins. (B) Gabbro with a hornblende and augite matrix, and plagioclase crystals. (C) Photomicrograph (XPL) of altered felsic rock with albite, quartz, hornblende, and calcite. (D) Photomicrograph (XPL) of gabbro, highlighting plagioclase crystals with hornblende, actinolite, and chlorite (E). Photomicrograph (XPL) of felsic rock showing feldspar and quartz phenocrysts in a albite and quartz matrix with calcite (F). Photomicrograph (XPL) of gabbro showing corroded augite alongside hornblende, chlorite, and

 doi:10.20944/preprints202508.1721.v1

albite. Abbreviations: Ab: albite; Act: actinolite; Aug: augite; Cc: calcite; Chl: chlorite; Hbl: hornblende; Kf: k-feldspar; Qz: quartz; Plg: plagioclase; XPL: crossed nicols.

5.3. Gabbro Dikes

Gabbro dikes are subparallel to the mineralized shear zone and show medium- to fine-grained phaneritic texture. Less altered gabbros exhibit ophitic to subophitic textures composed of plagioclase and pyroxene. Increased alteration results in mineral assemblage dominated by amphiboles, albite, and chlorite.

6. Hydrothermal Alterations

The alteration sequence recognized at Antas Norte comprises:

- **Sodic alteration**: Dominated by albite replacement, pervasive in host rocks, particularly in felsic volcanics.
- **Potassic alteration**: Characterized by biotite and scapolite replacing amphiboles and feldspars, centered around mineralized zones.
- **Calcic alteration**: Marked by amphibole (hornblende, actinolite) and apatite formation, closely associated with copper mineralization.
- **Silicification**: Pervasive quartz veining and replacement, overprinting previous alteration stages.
- **Propylitic alteration**: Development of chlorite, epidote, and calcite, particularly at the periphery of ore zones.

The progressive evolution from sodic to calcic assemblages suggests cooling and decreasing salinity of hydrothermal fluids during the mineralization process.

Distal zones primarily exhibit sodic and potassic alterations. Sodic alteration forms albite (Figure 5A), with minor quartz and ilmenite (Figure 5A). Potassic alteration forms biotite (Figure 5B) and scapolite (Figure 5B). Proximal zones are dominated by calcic alteration, marked by amphiboles (Figure 5C) and apatite (Figure 5C). Mineralized breccia bodies (Figure 5E and 5F) contain altered rock clasts surrounded by a sulfide matrix, predominantly chalcopyrite (Figure 5D).

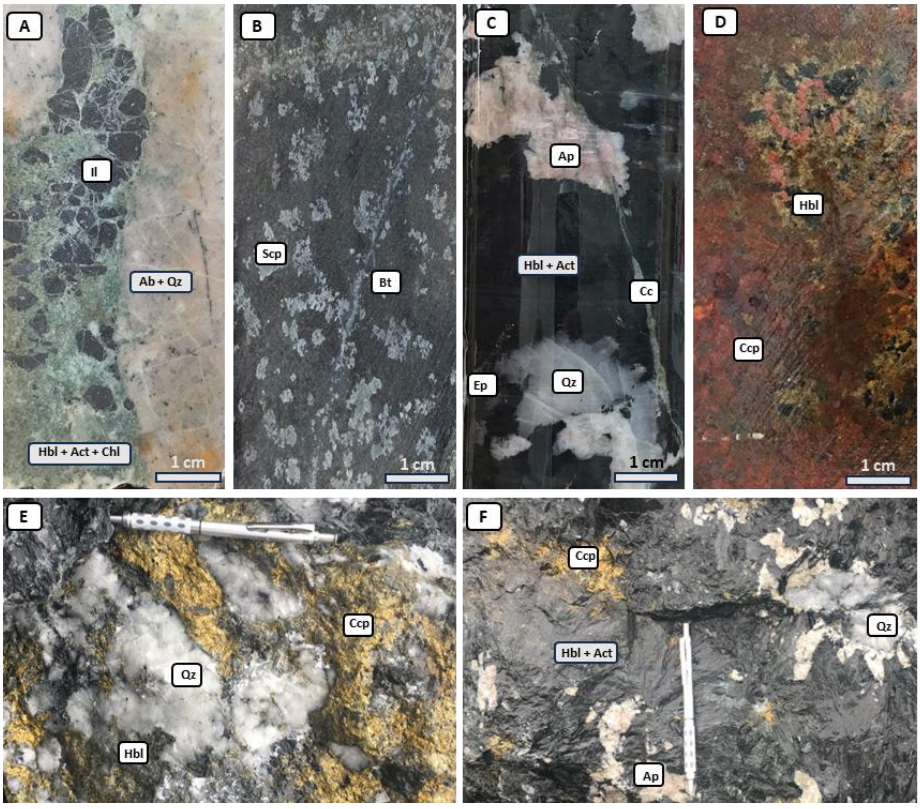

 doi:10.20944/preprints202508.1721.v1

Figure 5. Silicification (Figure 5A, 5C, 5E, 5F) is pervasive, varying in intensity across alterations. Propylitic alteration, characterized by chlorite (Figure 5A), epidote, and calcite (Figure 5C), is a late-stage overprint. **Abbreviations:** Ab: albite; Act: actinolite; Ap: apatite; Bt: biotite; Cc: calcite; Chl: chlorite; Ccp: chalcopyrite; Ep: epidote; Hbl: hornblende; Il: ilmenite; Qz: quartz; Scp: scapolite.

Figure 6 shows hydrothermal Alterations in the Antas Norte Area, Focusing on Sodic and Potassic Alterations (Figs A, B, C, D, E, F, G, H and I).

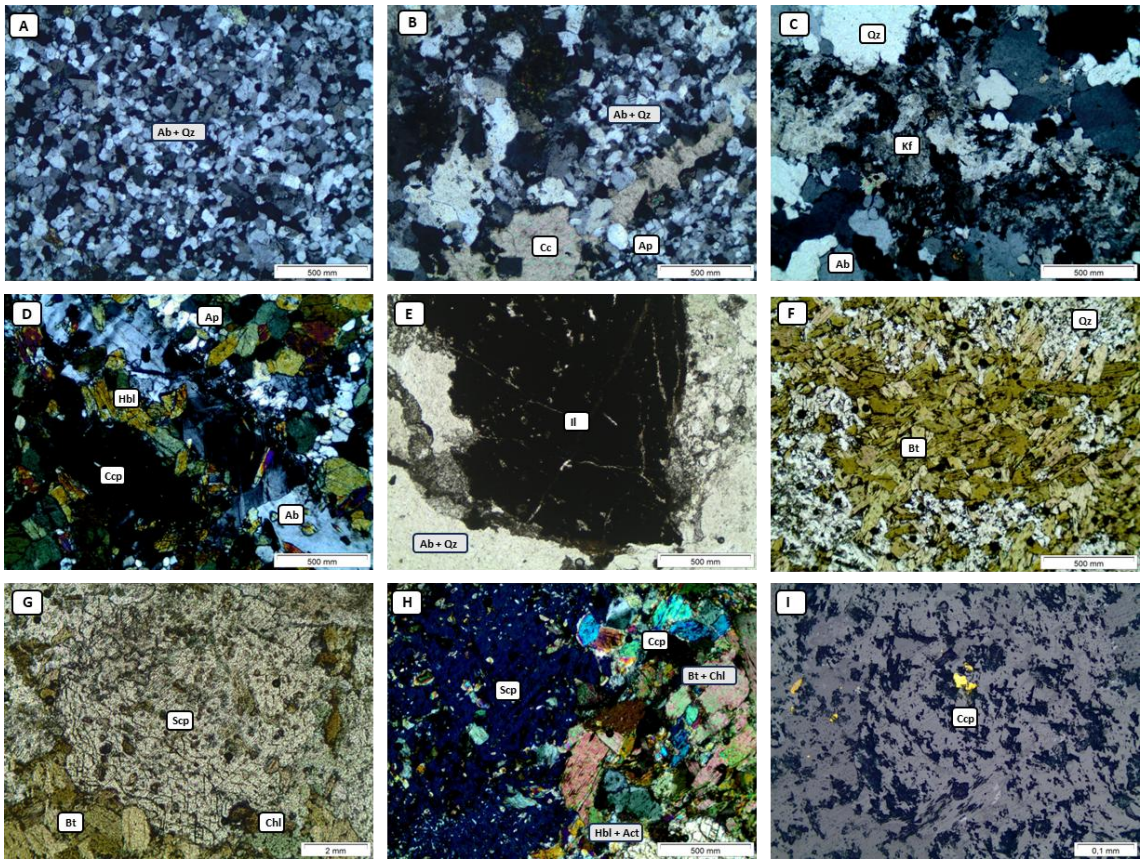

Figure 6. Hydrothermal Alterations in the Antas Norte Area, Focusing on Sodic and Potassic Alterations. (A) Photomicrograph (transmitted light—XPL) of the sodic alteration portion, with the fine matrix primarily formed by albite and quartz, the latter being a silicification product . (B) Photomicrograph (transmitted light—XPL) of the sodic alteration portion, with the medium matrix formed by albite and quartz, but with calcite filling a vein and small apatite crystals . (C) Photomicrograph (transmitted light—XPL) showing cloudy K-feldspar crystals alongside albite and quartz. (D) Photomicrograph (transmitted light—XPL) of the interaction between sodic and calcic alterations near mineralization, with albite representing the sodic alteration, hornblende and apatite representing the calcic alteration, and chalcopyrite (opaque) representing the mineralization. (E) Photomicrograph (transmitted light—PPL) of an ilmenite crystal bordered by a albite and quartz matrix. (F) Photomicrograph (transmitted light—PPL) of a biotite aggregate, the main characteristic of potassic alteration, with dispersed quartz crystals. (G) Photomicrograph (transmitted light—PPL) of a scapolite porphyroblast bordered by a biotite assemblage representing the mineral association of potassic alteration. Incipient chlorite alters the biotite. (H) Photomicrograph (transmitted light—XPL) showing the incipient interaction between potassic and calcic alterations, with scapolite and biotite crystals in contact with hornblende, actinolite, and chalcopyrite. Chlorite is observed altering biotite edges . (i) Photomicrograph (reflected light—PPL) of a biotite mass with chalcopyrite crystals due to the proximity to mineralization.

 doi:10.20944/preprints202508.1721.v1

7. Mineralization

Copper mineralization at the Antas Norte deposit is hosted within the mafic and felsic metavolcanic rocks of the Grão Pará Group and is spatially associated with calcic hydrothermal alteration (hornblende–apatite–allanite–titanite assemblage). The mineralized body exhibits a subvertical dip towards the southeast and shows NE–SW trend, paralleling the shear zone controlling the deposit.

Mineralization occurs in three principal styles:

1. **Massive sulfide ore**: Dominant in the central portions of the orebody, primarily composed of chalcopyrite with subordinate pyrrhotite and pyrite.
2. **Brecciated sulfide ore**: Present along the margins of massive zones, associated with brecciated hydrothermalized host rocks, where sulfides infill breccia matrices.
3. **Veins and veinlets**: Less volumetrically significant, predominantly composed of chalcopyrite, pyrrhotite, and minor ilmenite, crosscutting earlier alteration zones.

The massive sulfide portions are dominated by chalcopyrite, with pyrrhotite and pyrite inclusions. Preserved cores of hydrothermal minerals, including hornblende, actinolite, and apatite, are observed within the sulfide mass, indicating overprinting of earlier alteration assemblages by mineralization.

Breccia zones exhibit matrix composed of chalcopyrite + pyrrhotite + pyrite ± ilmenite ± sphalerite ± pentlandite ± hornblende ± actinolite ± quartz ± apatite ± chlorite ± epidote ± albite. Chalcopyrite dominates the matrix, while hydrothermal clasts of hornblende, actinolite, and quartz occur as angular to rounded fragments.

Veins and veinlets, predominantly composed of chalcopyrite with minor pyrrhotite and ilmenite, are observed crosscutting both calcareous and sodic alteration zones. Gabbro dikes that intersect the ore zone show minimal sulfide mineralization, suggesting post-mineralization emplacement or weak mineralizing fluid interaction.

Massive ore at the body core (Figure 7A). 2. Brecciated ore at the edges, interacting with hydrothermal alterations (Figure 7B). 3. Veins and veinlets, which are less expressive (Figure 7C).

The mineralization is associated with a ductile-brittle regime, where the central zones remain undeformed, while brecciation affects the edges. The presence of gold is inferred from chemical analyses, as it was not identified in petrographic slides.

In massive sulfide portions, chalcopyrite dominates (Figure 7D, &E), with inclusions of pyrrhotite (Figure 7E), pyrite (Figure 7D), and sphalerite (Figure 7E). These zones envelop areas of prior alteration, where hornblende, actinolite, and apatite cores are preserved (Figure 7F).

Breccias show mineral association of chalcopyrite + pyrrhotite + pyrite ± ilmenite + sphalerite ± pentlandite + hornblende + actinolite ± quartz + apatite ± chlorite ± epidote ± albite. Chalcopyrite dominates the breccia matrix (Figure 7G, 7H, 7I,7J)), with accessory phases including pyrrhotite (Figure 7K), pyrite, ilmenite (Figure 7J), sphalerite, and pentlandite. Hydrothermal minerals such as hornblende (Figure 7H, 7I), actinolite (Figure 7H, 7I), quartz (Figure 7I), and apatite form angular to rounded clasts. Chlorite (Figure 7H) and epidote (Figure 7H) appear in areas of propylitic alteration, while albite (Figure 8I) occurs at contacts between calcic and sodic alteration zones.

 doi:10.20944/preprints202508.1721.v1

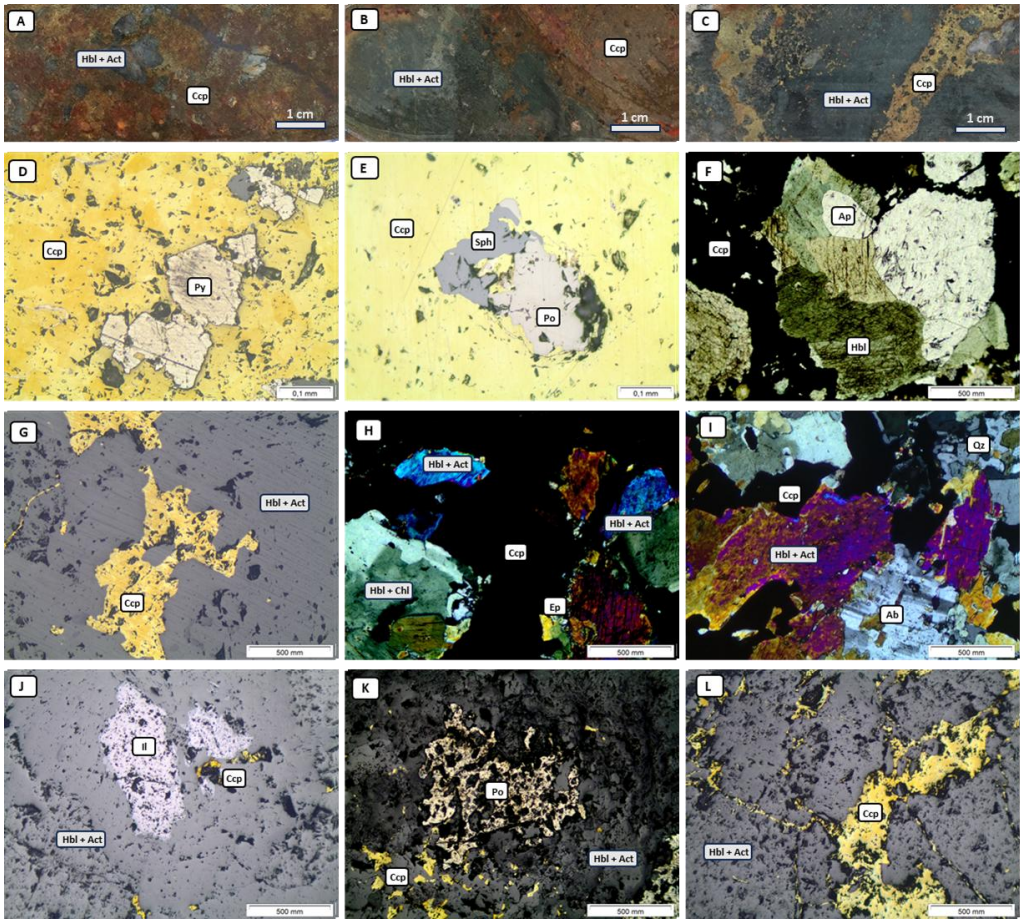

Figure 7. Illustrates mineralized zones, photomicrographs of sulfide textures, and alteration phases: **Abbreviations:** Ab: albite; Act: actinolite; Ap: apatite; Ccp: chalcopyrite; Chl: chlorite; Ep: epidote; Hbl: hornblende; Il: ilmenite; Qz: quartz; Po: pyrrhotite; Py: pyrite; Sph: sphalerite; XPL: cross polarized light; PPL: plane polarized light.

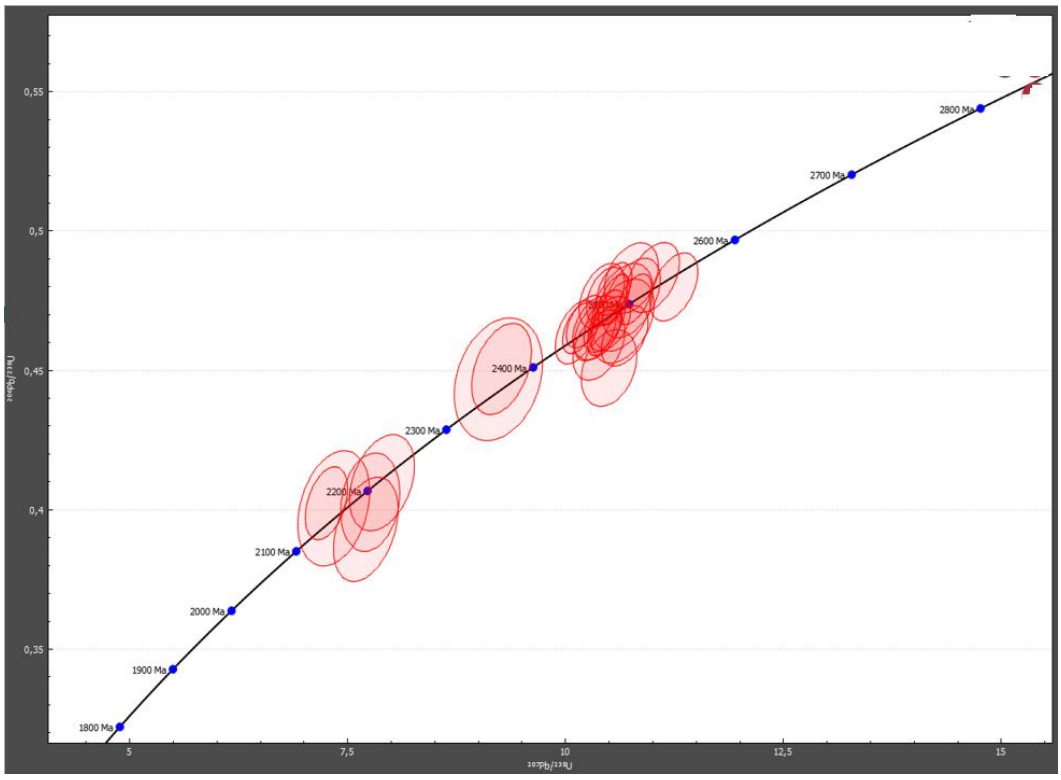

 doi:10.20944/preprints202508.1721.v1

Figure 8. Concordia diagram of U-Pb isotopic data for hydrothermal titanite from the Antas Norte deposit. Two distinct concordant age populations are observed at approximately 2.50 Ga and 2.20 Ga, indicating multiple hydrothermal events related to Archean and Paleoproterozoic tectonothermal episodes. Error ellipses are shown at 2σ confidence level.

8. Geocronology

The U-Pb isotopic dating of hydrothermal titanite from the Antas Norte deposit yielded two significant concordant age populations. Analyses show ages around **2.50 Ga** and **2.20 Ga**, corresponding to two distinct tectonothermal events affecting the region. The older population (~2.50 Ga) likely shows an early hydrothermal alteration event during late Archean crustal processes, while the younger age (~2.20 Ga) corresponds to a major Paleoproterozoic tectonothermal reactivation. These results confirm that the copper mineralization was associated with multiple fluid flow episodes linked to the regional deformation history. The high degree of concordance between 206Pb/238U and 207Pb/235U systems in titanite grains supports the robustness of these ages for constraining the timing of mineralization and associated hydrothermal events at Antas Norte.

9. Structural Geology

The Carajás Mineral Province has undergone multiple tectonic events from the Archean to the Paleoproterozoic, imprinting a complex network of ductile to brittle structures. Regional tectonics are dominated by the Carajás Transcurrent System, characterized by NW–SE trending shear zones that exert strong control over ore localization.

At Antas Norte, the mineralized body is hosted within a secondary NE–SW-oriented shear zone, distinct from the major Carajás Fault (WNW–ESE orientation). The shear zone exhibits features typical of a dextral transpressional regime, with deformation patterns transitioning from ductile to brittle conditions.

Structural analysis reveals two foliation generations :

- **Sn foliation**: A pervasive mylonitic foliation defined by the preferred orientation of amphiboles, plagioclase, and biotite, which trends NNE–SSW and dips ESE.
- **Sn+1 foliation**: A later foliation characterized by the alignment of hydrothermal minerals, particularly oriented mafic minerals surrounding quartz and feldspar porphyroclasts, which trends ENE–WSW and dips SSE.

The orebody is located along a sigmoidal SC (Shear–C) structure, where mineralized zones are concentrated in dilational spaces between Sn and Sn+1 foliations. Stretching lineation measurements indicate a plunge of 54° towards 225° (SW), which is consistent with the orientation of high-grade mineralization zones (Figure 9).

Hydrothermal fluids exploited these deformation zones, resulting in intense alteration and mineral precipitation along the structural conduits.

 doi:10.20944/preprints202508.1721.v1

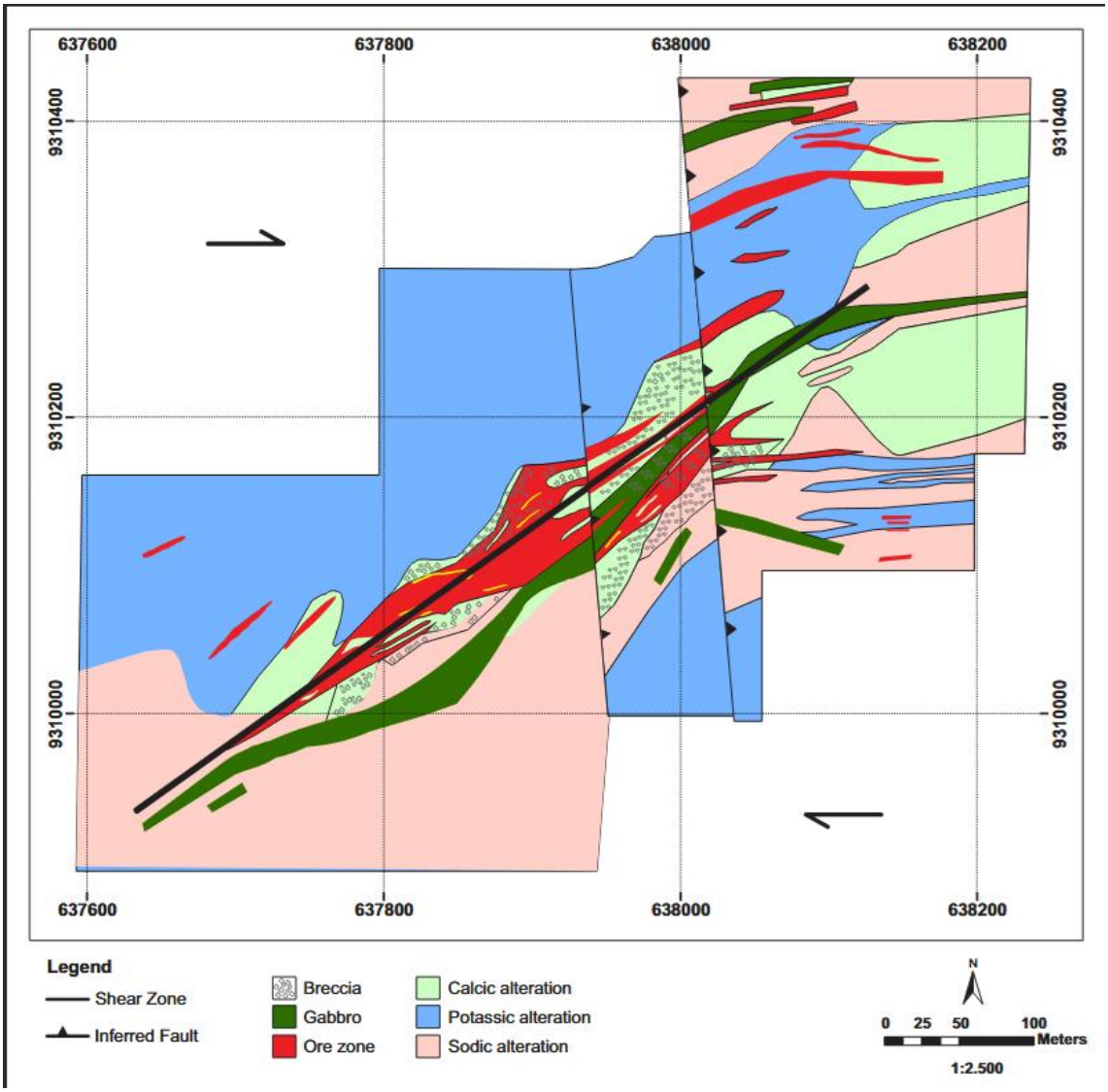

Figure 9. Hydrothermal alteration map of the Antas Norte mine with SC structure (Modified from Oz Minerals internal files). (A) Sn Foliation: Defined by amphiboles, plagioclases, and biotite, trending NNE-SSW and dipping ESE . (B) Sn+1Foliation: Associated with hydrothermal minerals, marked by oriented mafic minerals surrounding quartz and feldspar porphyroclasts. This foliation trends ENE-WSW and dips SSE.

10. 3D Geological Modeling

The 3D geological modeling of the Antas Norte deposit was developed using an implicit modeling approach using the Leapfrog Geo 2022 software. The model was constructed by integrating geological surface maps, drill hole data (totaling 30,657.55 meters), detailed topographic surveys, and structural measurements.

The results highlight that the mineralized body is spatially controlled by a NE–SW-trending shear zone. Secondary NNW–SSE-oriented faults were identified, offsetting the mineralized zones laterally. These structures were crucial for understanding the orebody geometry and its internal segmentation.

The mineralization is associated with a major subvertical tabular body that trends NE–SW, dipping steeply southeast, and is aligned with the primary shear zone. High-grade massive sulfides (>3% Cu) occur in the body core , surrounded by lower-grade disseminated mineralization (<3% Cu).

Hydrothermal alterations are spatially zoned:

- Sodic alteration (albite) dominates at regional scale;
- Potassic alteration (biotite + scapolite) surrounds the mineralized core;

 doi:10.20944/preprints202508.1721.v1

- Calcic alteration (amphibole + apatite) is closely associated with copper mineralization.

Silicification and propylitic alteration were pervasive but diffuse and, therefore, were not modeled as discrete solids.

The shear zone acted as the primary conduit for hydrothermal fluids, controlling both the localization and morphology of mineralized zones. The 3D model provides critical insights into the hydrothermal fluid flow pathways and the spatial distribution of metal precipitation within the structural framework (Figure 10).

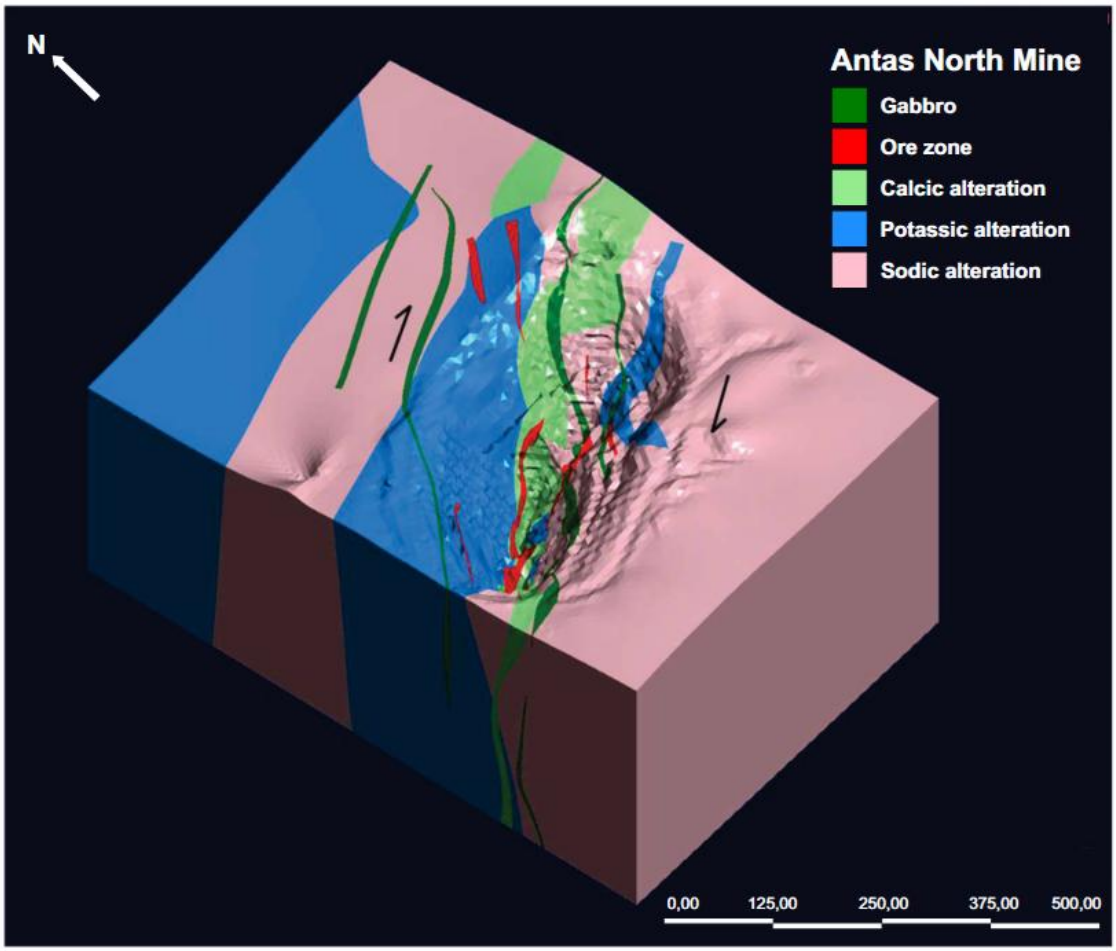

Figure 10. 3D model of the Antas Norte mine, showing the entire set of alterations, the mineralized body, and the extraction pit.

11. Discussion

The Antas Norte deposit exhibits a distinctive mineralogical and structural signature compared to most Iron Oxide Copper-Gold (IOCG) deposits in the Carajás Mineral Province. Unlike classic IOCG deposits such as Salobo and Sossego, which are typically associated with extensive iron oxide (magnetite and/or hematite) mineralization, Antas Norte is characterized by the dominance of iron sulfides (pyrrhotite and pyrite) and ilmenite.

The spatial mineralization association with secondary NE–SW-oriented shear zone highlights the critical role of structural controls in focusing hydrothermal fluids. The evolution of hydrothermal alteration, progressing from early sodic (albite-rich) to later potassic (biotite + scapolite) and calcic (amphibole + apatite) assemblages, reflects a dynamic fluid regime with decreasing temperature, salinity, and pH over time. The presence of widespread silicification and propylitic alteration suggests the late influx of meteoric fluids during shear zone reactivation.

 doi:10.20944/preprints202508.1721.v1

The mineralogical assemblages at Antas Norte imply hydrothermal conditions significantly different from those prevailing in the more oxidized IOCG systems of Carajás. Specifically, the stability of ilmenite rather than magnetite indicates formation under lower oxygen fugacity (fO_2) conditions. Ilmenite stability at deeper crustal levels has been reported in other iron oxide–apatite (IOA) systems worldwide, where reduced magmatic conditions promote titanium retention and iron sulfide over iron oxide mineralization.

These features suggest that Antas Norte represents a deeper, more reduced end-member within the IOCG mineralization spectrum of Carajás. Such an interpretation is consistent with recent models proposing that IOCG and ISCG deposits form a continuum related to variations in redox state, fluid composition, and crustal depth.

Therefore, the Antas Norte deposit provides important insights into the diversity of mineral systems in the Carajás Province, highlighting the influence of structural reactivation, fluid evolution, and redox controls on deposit genesis.

12. Conclusions

The Antas Norte deposit represents a distinct copper-gold mineralization style within the Carajás Mineral Province, characterized by the predominance of iron sulfides (pyrrhotite, pyrite) and ilmenite rather than iron oxides.

Three main mineralization styles were identified:

- Massive sulfide bodies,
- Breccia matrix sulfide infill,
- Sulfide veins and veinlets.

These mineralization styles are spatially and genetically associated with calcic hydrothermal alteration and localized within a NE–SW-trending shear zone, evidencing the critical role of structural controls on fluid flow and ore deposition.

The hydrothermal evolution of Antas Norte, from sodic to potassic to calcic alteration assemblages, reflects a dynamic fluid system with progressive changes in temperature, salinity, and pH. The stability of ilmenite and dominance of iron sulfides over iron oxides indicate a reduced hydrothermal environment, contrasting with the more oxidized conditions typical of classic IOCG systems in Carajás.

The integration of field observations, petrography, structural analysis, and 3D geological modeling supports the interpretation of Antas Norte as a deeper, more reduced end-member of the IOCG mineralization spectrum. This study contributes to a better understanding of the diversity of mineralization styles in Carajás and emphasizes the need for refined exploration models considering structural and redox variations across the province.

References

1. Araújo, O. J. B. & Maia, R. G. N. 1991. Serra dos Carajás, folha SB.22-ZA, Estado do Pará. Programa Levantamentos Geológicos Básicos do Brasil. Companhia de Pesquisa de Recursos Minerais. 136.
2. Araújo, O. J. B., Maia, R. G. N., Jorge-João, X. S. & Costa, J. B. S. 1988. A megaestruturação da folha Serra dos Carajás. In: Congr. Latino-Americano de Geologia, 7, Proceedings, 324–333.
3. Arias, M., Nuñez, P., Arias, D., Gumiel, P., Castañón, C., Fuertes-Blanco, J. & Martin-Izard, A. 2021. 3D Geological Model of the Touro Cu Deposit, A World-Class Mafic-Siliciclastic VMS Deposit in the NW of the Iberian Peninsula. Minerals, 11: 85. https://doi.org/10.3390/min11010085
4. Augusto, R. A., Monteiro, L. V. S., Xavier, R. & Souza Filho, C. R. 2008. Zonas de alteração hidrotermal e paragênese do minério de cobre do Alvo Bacaba, Província Mineral de Carajás (PA). Revista Brasileira de Geociências, 38: 263–277.
5. Avelar, V. G., Lafon, J. M., Correia Jr, F. C. & Macambira, E. M. B. 1999. O magmatismo arqueano da região de Tucumã—Província Mineral De Carajás: Novos resultados geocronológicos. Revista Brasileira de Geociências, 29: 453–460.

 doi:10.20944/preprints202508.1721.v1

6. Barros, C. E. M., Dall'Agnol, R., Barbey, P. & Boullier, A. M. 1997. Geochemistry of the Estrela Granite Complex, Carajás region, Brazil: an example of an Archaean A-type granitoid. Journal of South American Earth Sciences, 10: 321–330.
7. Barros, C. E. M., Macambira, M. J. B., Barbey, P. & Scheller, T. 2004. Dados isotópicos Pb-Pb em zircão (evaporação) e Sm-Nd do Complexo Granítico Estrela, Província Mineral de Carajás, Brasil: Implicações petrológicas e tectônicas. Revista Brasileira de Geociências, 34: 531–538.
8. Barton, M. D. 2013. Iron Oxide(-Cu-Au-REE-P-Ag-U-Co) Systems. In Treatise on Geochemistry: Second Edition, 13, 515–541. Elsevier Inc. https://doi.org/10.1016/B978-0-08-095975-7.01123-2
9. Barton, M. D. & Johnson, D. A. 2004. Footprints of Fe-oxide(-Cu-Au) systems. In SEG 2004: Predictive Mineral Discovery Under Cover. Centre for Global Metallogeny, Spec. Pub. 33, The University of Western Australia, 112–116.
10. Botelho, N. F., Moura, M. A., Teixeira, L. M., Olivo, G. R., Cunha, L. M. & Santana, M. U. 2005. Caracterização geológica e metalogenética do depósito de Cu ± (Au, W, Mo, Sn) Breves, Carajás. In: Marini OJ, Queiroz ET, Ramos BW (eds). Caracterização do Depósitos Minerais em Distritos Mineiros da Amazônia. DMNP-CT-mineral / FINEPADIMB, 339–389.
11. Buddington, A. F. & Lindsley, D. H. 1964. Iron-titanium oxide minerals and synthetic equivalents. Journal of Petrology, 5: 310–357.
12. Case, G., Blenkinsop, T., Chang, Z., Huizenga, J. M., Lilly, R. & McLellan, J. 2017. Delineating the structural controls on the genesis of iron oxide–Cu–Au deposits through implicit modelling: a case study from the e1 group, Cloncurry district, Australia. Geological Society, London, Special Publications, 453, 1: 349–384. https://doi.org/10.1144/sp453.4
13. Corriveau, L. 2007. Iron oxide copper-gold deposits: A Canadian perspective. In W. D. Goodfellow (ed.), Mineral Deposits in Canada: A Synthesis of Major Deposit Types, District Metallogeny, the Evolution of Geological Provinces and Exploration Methods, 307–328.
14. Craveiro, G. S., Villas, R. N., & Costa Silva, A. R. 2012. Depósito Cu-Au Visconde, Carajás (PA): geologia e alteração hidrotermal das rochas encaixantes. Revista Brasileira de Geociências, 42(3): 453–470.
15. Craveiro, G. S., Xavier, R. P. & Villas, R. N. N. 2019. The Cristalino IOCG deposit: an example of multi-stage events of hydrothermal alteration and copper mineralization. Brazilian Journal of Geology, 49(1): 1–18.
16. Docegeo. 1988. Revisão litoestratigráfica da Província Mineral de Carajás—Litoestratigrafia e principais depósitos minerais. In: Cong. Bras. Geol., 35, SBG, 11–54.
17. Domingos, F. H. G. 2009. The Structural Setting of the Canaã dos Carajás Region and Sossego-Sequeirinho Deposits, Carajás Brazil. Doctor of Philosophy thesis. University of Durham, Durham, 483.
18. Feio, G. R. L., Dall'Agnol, R., Dantas, E. L., Macambira, M. J. B., Gomes, A. C. B., Sardinha, A. S., Oliveira, D. C., Santos, R. D. & Santos, P. A. 2012. Geochemistry, geochronology, and origin of the Neoarchean Planalto Granite suite, Carajás, Amazonian craton: A-type or hydrated charnockitic granites? Lithos, 151: 57–73.
19. Feio, G. R. L., Dall'Agnol, R., Dantas, E. L., Macambira, M. J. B., Santos, J. O. S., Althoff, F. J. & Soares, J. E. B. 2013. Archean granitoid magmatism in the Canaã dos Carajás area: Implications for crustal evolution of the Carajás province, Amazonian craton, Brazil. Precambrian Research, 227: 157–185.
20. Ferreira Filho, C. F., Cançado, F., Correa, C., Macambira, E. M. B., Junqueira-Brod, T. C. & Siepierski, L. 2007. Mineralizações estratiformes de PGE-Ni associadas a complexos acamadados em Carajás: os exemplos de Luanga e Serra da Onça. In: Rosa-Costa L.T., Klein E.L., Viglio E.P. (eds.). Contribuições à Geologia da Amazônia. SBG-Núcleo Norte, Belém, p. 1–14.
21. Fournier, R. O. 1983. Active hydrothermal systems as analogues of fossil systems. In: Eaton, G., (eds.). The Role of Heat in the Development of Energy and Mineral Resources in the Northern Basin and Range Province. Geothermal Resources Council Special Report, 13: 263–284.
22. Galarza, M. A., Macambira, M. J. B. and Moura, C. A. V. 2003. Geocronologia Pb-Pb e Sm–Nd das rochas máficas do depósito Igarapé Bahia, Província Mineral de Carajás (PA). 7º Simpósio de Geologia da Amazônia, [CD-ROM].

 doi:10.20944/preprints202508.1721.v1

23. Garcia, V. B., Schutesky, M. E., Oliveira, C. G., Whitehouse, M. J., Hühn, S. R. B. and Augustin, C. T. 2020. The Neoarchean GT-34 Ni deposit, Carajás mineral Province, Brazil: An atypical IOCG-related Ni sulfide mineralization. Ore Geology Reviews, 127:103773. https://doi.org/10.1016/j.oregeorev.2020.103773.
24. Giustina, M. E. S. D. and Oliveira, C. G. 2020. From the roots to the roof? A verticalization model for the Carajás IOCG Province, Brazil. Ore Geology Reviews, 127.
25. Grainger, C. J., Groves, D. I., Tallarico, F. H. B. and Fletcher, I. R. 2008. Metallogenesis of the Carajás Mineral Province, Southern Amazon Craton, Brazil: Varying styles of Archean through Paleoproterozoic to Neoproterozoic base- and precious-metal mineralization. Ore Geology Reviews, 33:451-489.
26. Groves, D. I., Bierlein, F. P., Meinert, L. D. and Hitzman, M. W. 2010. Iron Oxide Copper-Gold (IOCG) Deposits through Earth History: Implications for Origin, Lithospheric Setting, and Distinction from Other Epigenetic Iron Oxide Deposits. Economic Geology, 105:641-654.
27. Haddad-Martim, P. M., Souza Filho, C. R. and Carranza, E. J. M. 2017. Spatial analysis of mineral deposit distribution: A review of methods and implications for structural controls on iron oxide-copper-gold mineralization in Carajás, Brazil. Ore Geology Reviews, 81(1):230-244. https://doi.org/10.1016/j.oregeorev.2016.09.038.
28. Haggerty, S. 1976. Opaque mineral oxides in terrestrial igneous rocks. Mineralogical Society of America. Short Course Notes, 3:101–300.
29. Haynes, D. W. 2000. Iron oxide copper (-gold) deposits: their position in the deposit spectrum and modes of origin. In Hydrothermal iron oxide copper-gold and related deposits. A global perspective, 1:71–90. Australian Mineral Foundation.
30. Hirata, W. K., Rigon, J. C., Kadekaru, K., Cordeiro, A. A. C. and Meireles, E. A. 1982. Geologia Regional da Província Mineral de Carajás. Simpósio de Geologia da Amazônia, 1st, Belém, Abstracts, 100-110.
31. Hitzman, M. W. 2000. Iron oxide-Cu-Au deposits: what, where, when and why? In T. M. Porter (Ed.), Hydrothermal iron oxide copper-gold and related deposits. A global perspective, Australian Mineral Foundation, 1:9–25.
32. Hitzman, M. W., Oreskes, N. and Einaudi, M. T. 1992. Geological characteristics and tectonic setting of Proterozoic iron oxide (Cu-U-Au-REE) deposits. Precambrian Research, 58:241–287.
33. Holdsworth, R. and Pinheiro, R. 2000. The anatomy of shallow-crustal transpressional structures: insights from the Archean Carajás fault zone, Amazon, Brazil. Journal of Structural Geology, 22:1105-1123.
34. Huang, X-W. and Beaudoin, G. 2019. Textures and Chemical Compositions of Magnetite from Iron Oxide Copper-Gold (IOCG) and Kiruna-Type Iron Oxide-Apatite (IOA) Deposits and Their Implications for Ore Genesis and Magnetite Classification Schemes. Economic Geology, 114(5):953–979. https://doi.org/10.5382/econgeo.4651.
35. Hühn, S. R. B., Silva, A. M., Ferreira, F. J. F. and Braitenberg, C. 2020. Mapping New IOCG Mineral Systems in Brazil: The Vale do Curaçá and Riacho do Pontal Copper Districts. Minerals, 10:1074. https://doi.org/10.3390/min10121074.
36. Hühn, S. R. B., Souza C. I. J., Albuquerque, M. C., Leal, E. D. and Brustolin, V. 1999a. Descoberta do depósito Cu (Au) Cristalino: Geologia e mineralização associada região da Serra do Rabo—Carajás—PA. In: Simpósio de Geologia da Amazônia, 6, Boletim de Resumos, 140–143.
37. Hühn, S. R. B., Macambira, M. J. B. and Dall'Agnol, R. 1999b. Geologia e geocronologia Pb-Pb do Granito Alcalino Planalto, Região da Serra do Rabo, Carajás-PA. In: Simpósio de Geologia da Amazônia, Boletim de Resumos, 6:463-466.
38. Hühn, S. R. B. and Nascimento, J. A. S. 1997. São os depósitos cupríferos de Carajás do tipo Cu-Au-U-ETR? In: Costa, M.L. & Angélica, R.S. (Eds.) Contribuições à Geologia da Amazônia. FINEP, SGB-NO, 143-160.
39. Kampmann, T. C., Stephens, M. B. and Weihed, P. 2016. 3D modelling and sheath folding at the Falun pyritic Zn-Pb-Cu-(Au-Ag) sulphide deposit and implications for exploration in a 1.9 Ga ore district, Fennoscandian Shield, Sweden. Mineral Deposita, 51:665–680.
40. Li, B., Peng, Y., Zhao, X., Liu, X., Wang, G., Jiang, H., Wang, H. and Yang, Z. 2022. Combining 3D Geological Modeling and 3D Spectral Modeling for Deep Mineral Exploration in the Zhaoxian Gold Deposit, Shandong Province, China. Minerals, 12:1272. https://doi.org/10.3390/min12101272.

 doi:10.20944/preprints202508.1721.v1

41. Lindenmayer, Z. G. and Teixeira, J. B. G. 1999. Ore genesis at the Salobo copper deposit, Serra dos Carajás. In: Silva M. G., Misi A. (eds.). Base Metal Deposits of Brazil. MME/CPRM/DNPM, Belo Horizonte, 33-43.
42. Lindenmayer, Z. G., Pimentel, M. M., Ronchi, L. H., Althoff, F. J., Laux, J. H., Araújo, J. C., Fleck, A., Baecker, C. A., Carvalho, D. B. and Nowatzki, A. C. 2001b. Geologia do depósito de Cu-Au de Gameleira Serra dos Carajás, Pará. In: Jost H., Brod J.A., Quieroz E.T. (eds.) Caracterização de depósitos auríferos em distritos mineiros brasileiros. Brasilia, ADIMB-DNPM, p. 79-139.
43. Lindenmayer, Z. G. 2003. Depósito de Cu–Au do Salobo, Serra dos Carajás: Uma revisão. In: L.H. Ronchi and F.J. Althoff (eds.). Caracterização e modelamento de depósitos minerais. São Leopoldo, Editora Unisinos, 69–98.
44. Lindenmayer, Z. G., Fleck, A., Gomes, C. H., Santos, A. B. S., Caron, R., Paula, F. C., Laux, J. H., Pimental, M. M. and Sardinha, A. S. 2005. Caracterização geológica do Alvo Estrela (Cu-Au), Serra dos Carajás, Pará. In: Marini OJ, Queiroz ET, Ramos BW (eds). Caracterização dos depósitos minerais em distritos mineiros da Amazônia. DMNPCT-mineral/FINEP-ADIMB, 157–225.
45. Macambira, E. B. M. and Ferreira Filho, C. F. 2005. Exploration and origin of stratiform PGE mineralization in the Serra da Onça layered complex, Carajás Mineral Province, Brazil. In: 10th International Platinum Symposium Extended Abstract, Oulu.
46. Macambira, E. B. M. and Ferreira Filho, C. F. 2002. Fracionamento magmático dos corpos máfico ultramáficos da Suíte Intrusiva Cateté—sudeste do Pará. In: Klein EL, Vasquez ML, Rosa-Costa LT (Eds) Contribuições à geologia da Amazônia. Belém, SBG-Núcleo Norte, 105-114.
47. Machado, N., Krough, T. E. and Lindenmayer, Z. G. 1991. U–Pb geochronology of Archean magmatism and basement reactivation in the Carajás Area, Amazon Shield, Brazil. Precambrian Res., 49:1-26.
48. Mansur, E. T., Ferreira Filho, C. F. and Oliveira, D. P. 2020. The Luanga deposit, Carajás Mineral Province, Brazil: Different styles of PGE mineralization hosted in a medium-size layered intrusion. Ore Geology Reviews, 118:103340.
49. Mansur, E. T., Ferreira Filho, C. F., 2016. Magmatic structure and geochemistry of the Luanga Mafic-Ultramafic Complex: Further constraints for the PGE-mineralized magmatism in Carajás, Brazil. Lithos. doi:10.1016/j.lithos.2016.09.036.
50. Martin-Izard, A., Arias, D., Arias, M., Gumiel, P., Sanderson, D.J., Castañón, C., Lavandeira, A. and Sanchez, J. 2015. A new 3D geological model and interpretation of structural evolution of the world-class Rio Tinto VMS deposit, Iberian Pyrite Belt (Spain). Ore Geol. Rev. 71: 457–476.
51. Marschik, R., Mathur, R., Ruiz, J., Leveille, R.A. and Almeida, A-J. 2005. Late Archean Cu-Au-Mo mineralization at Gameleira and Serra Verde, Carajás Mineral Province, Brazil: constraints from Re-Os molybdenite ages. Mineralium Deposita, 39:983-991.
52. Melo, G. H. C., Monteiro, L. V. S., Moreto, C. P. N., Xavier, R. P. and Silva, M. A. D. 2014. Paragenesis and evolution of the hydrothermal Bacuri iron oxide-copper-gold deposit, Carajás Province (PA). Brazilian Journal of Geology, [S.L.], 44(1):73-90. FapUNIFESP (SciELO). http://dx.doi.org/10.5327/z2317-4889201400010007
53. Melo, G. H. C. 2011. Contexto geológico e evolução metalogenética do depósito de cobre Bacuri, Província Mineral de Carajás. Trabalho de Conclusão de Curso, Instituto de Geociências, Universidade de Campinas, 66.
54. Monteiro, L. V. S., Xavier, R. P., Carvalho, E. R., Hitzman, M. W., Johnson, C. A., Souza Filho, C. R. and Torresi, I. 2008a. Spatial and temporal zoning of hydrothermal alteration and mineralization in the Sossego iron oxide-copper-gold deposit, Carajás Mineral Province, Brazil: Paragenesis and stable isotope constraints. In Mineralium Deposita, 43(2). https://doi.org/10.1007/s00126-006-0121-3
55. Monteiro, L. V. S., Xavier, R. P., Hitzman, M. W., Juliani, C., Souza Filho, C. R. and Carvalho, E. R. 2008b. Mineral chemistry of ore and hydrothermal alteration at the Sossego iron oxide–copper–gold deposit, Carajás Mineral Province, Brazil. Ore Geology Reviews, 34:317-336.
56. Monteiro, L. V. S., Xavier, R. P., Souza Filho, C. R. and Augusto, R. A. 2007. Aplicação de isótopos estáveis ao estudo dos padrões de distribuição das zonas de alteração hidrotermal associados ao sistema de óxido de ferro-cobre-ouro Sossego, Província Mineral de Carajás. In: Congresso Brasileiro de Geoquímica. Atibaia, Sociedade Brasileira de Geoquímica.

 doi:10.20944/preprints202508.1721.v1

57. Moreto, C. P. N., Monteiro, L. V. S., Xavier, R. P., Creaser, R. A., Dufrane, S. A., Tassinari, C. C. G., Sato, K. 2015a. Timing of multiple hydrothermal events in the iron oxide–copper–gold deposits of the Southern Copper Belt, Carajas Province, Brazil. Mineralium Deposita, 50(5):517-546. https://doi.org/10.1007/s00126-014-0549-9
58. Moreto, C. P. N., Monteiro, L. V. S., Xavier, R. P., Creaser, R. A., Dufrane, S. A., Tassinari, C. C. G., Sato, K., Kemp, A. I. S., Amaral, W. S. 2015b. Neoarchean and Paleoproterozoic iron oxide-copper-gold events at the Sossego deposit, Carajas Province, Brazil, Re-Os and U-Pb geochronological evidence. Economic Geology, 110(3):809-835. https://doi.org/10.2113/econgeo.110.3.809
59. Moreto, C. P. N. 2013. Geocronologia U-Pb e Re-Os aplicada à evolução metalogenética do Cinturão Sul do Cobre da Província Mineral de Carajás. Tese de Doutorado, Instituto de Geociências, UNICAMP, 216.
60. Moreto, C. P. N., Monteiro, L. V. S., Xavier, R. P., Amaral, W. S., Santos, J. S. S., Juliani, C., Souza Filho, C. R. 2011. Mesoarchean (3.0 and 2.86 Ga) host rocks of the iron oxide-Cu-Au Bacaba deposit, Carajás Mineral Province: U-Pb geochronology and metallogenetic implications. Mineralium Deposita, 46:789-811. https://link.springer.com/article/10.1007/s00126-011-0352-9
61. Nogueira, A. C. R., Truckenbrodt, W., Pinheiro, R. V. L. 1995. Formação Águas Claras, Pré-Cambriano da Serra dos Carajás: redescrição e redefinição litoestratigráfica. Bol. Mus. Par. Em. Goeldi. Ciência da Terra, 7: 177-277.
62. Oliveira, C. G., Santos, R. V., Lafon, J. M. 1994. Variação da razão 87Sr/86Sr durante a evolução da zona de cisalhamento aurífera de Diadema, Sudeste do Pará. In: 38 Congresso Brasileiro de Geologia, Camboriú. Resumos Expandidos, 2:415-416.
63. Oz Minerals. 2020. Antas North. Mineral Resource and Ore Reserve Statement and Explanatory Notes.
64. Oz Minerals. 2022. Pedra Branca. Mineral Resource and Ore Reserve Statement and Explanatory Notes.
65. Passchier, C. W., Trouw, R. A. J. 2005. Microtectonics. Berlin; New York, Springer.
66. Pestilho, A. L. S., Monteiro, L. V. S., Melo, G. H. C., Moreto, C. P. N., Juliani, C., Fallick, A. E., Xavier, R. P. 2020. Stable isotopes and fluid inclusion constraints on the fluid evolution in the Bacaba and Castanha iron oxide-copper-gold deposits, Carajás Mineral Province, Brazil. Ore Geology Reviews, 121:103738.
67. Pidgeon, R. T., Macambira, M. J. B., Lafon, J. M. 2000. Th-U-Pb isotopic systems and internal structures of complex zircons from an enderbite from the Pium Complex, Carajás province, Brazil: Evidence for the ages of granulite facies metamorphism and the protolith of the enderbite. Chem. Geol., 166:159–171.
68. Pimentel, M. M., Lindenmayer, Z. G., Laux, J. H., Armstrong, R., Araújo, J.C. 2003. Geochronology and Nd geochemistry of the Gameleira Cu–Au deposit, Serra dos Carajás, Brazil: 1.8–1.7 Ga hydrothermal alteration and mineralization. Journal of South American Earth Science, 15:803-813.
69. Pinheiro, R. V. L., Kadekaru, K., Soares, A. V., Freitas, C., Ferreira, S. N., Matos, F. M. V. 2013. Carajás, Brazil—a short tectonic review. In: XIII Simpósio de Geologia da Amazônia. Belém, 1086–1089.
70. Pinheiro, R. V. L., Holdsworth, R. E. 1997a. Reactivation of Archean strike-slip fault systems, Amazon region, Brazil. Journal of the Geological Society, 154: 99-103.
71. Pinheiro, R. V. L., Holdsworth, R. E. 2000. Evolução tectonoestratigráfica dos sistemas transcorrentes Carajás e Cinzento, Cinturão Itacaiúnas, na borda leste do Cráton Amazônico. Pará. Rev. Bras. Geociências, 30:597–606.
72. Pollard, P. J., Taylor, R. G., Peters, L., Matos, F., Freitas, C., Saboia, L., Huhn, S. R. B. 2018. 40Ar-39Ar dating of Archean iron oxide Cu-Au and Paleoproterozoic granite-related Cu-Au deposits in the Carajás Mineral Province, Brazil: implications for genetic models. Miner. Deposita, 1–18.
73. Reed, M. H. 1997. Hydrothermal alteration and its relationship to ore fluid composition. In: Barnes H.L. (ed.). Geochemistry of Hydrothermal Ore Deposits, Wiley, New York, 303–365.
74. Réquia, K., Stein, H., Fontboté, L., Chiaradia, M. 2003. Re–Os and Pb–Pb geochronology of the Archean Salobo iron oxide copper–gold deposit, Carajás Mineral Province, northern Brazil. Mineralium Deposita, 38:727–738.
75. Rigon, J. C., Munaro, P., Santos, L. A., Nascimento, J. A. S. and Barreira, C. F. (2000) Alvo 118 copper–gold deposit: geology and mineralization, Serra dos Carajás, Pará, Brazil. 31st International Geological Congress, Rio de Janeiro. SBG, Abstract Volume, [CD-ROM].

 doi:10.20944/preprints202508.1721.v1

76. Rimstidt, J. D. (1997) Gangue mineral transport and deposition. In: Barnes, H. L. (ed.) Geochemistry of Hydrothermal Ore Deposits, 3rd ed. Wiley, New York, pp. 435–487.
77. Roberts, D. E. and Hudson, G. R. T. (1983) The Olympic Dam copper-uranium-gold deposit, Roxby Downs, South Australia. Economic Geology, 78, 799–822.
78. Rodriguez-Mustafa, M. A., Simon, A. C., Real, I., Thompson, J. F. H., Bilenker, L. D., Barra, F., Bindeman, I. and Cadwell, D. (2020) A Continuum from Iron Oxide Copper-Gold to Iron Oxide-Apatite Deposits: evidence from Fe and O stable isotopes and trace element chemistry of magnetite. Economic Geology, 115(7), 1443-1459. https://doi.org/10.5382/econgeo.4752.
79. Santos, J. O. S. (2003) Geotectônica do Escudo das Guianas e Brasil-Central. In: Bizzi, L.A. (ed.) Geologia, Tectônica e Recursos Minerais do Brasil: Texto, Mapas e SIG. CPRM, Brasília, pp. 169–226.
80. Sardinha, A. S., Barros, C. E. M. and Krymsky, R. (2006) Geology, geochemistry, and U-Pb geochronology of the Archean (2.74 Ga) Serra do Rabo granite stocks, Carajás Metallogenetic Province, northern Brazil. Journal of South American Earth Sciences, 20, 327–339.
81. Simon, A. C., Knipping, J., Reich, M., Barra, F., Deditius, A. P., Bilenker, L. and Childress, T. (2018) Kiruna-type iron oxide-apatite (IOA) and iron oxide copper-gold (IOCG) deposits form by a combination of igneous and magmatic-hydrothermal processes: Evidence from the Chilean iron belt. Society of Economic Geologists, Special Publication, 21, 89-114.
82. Siepierski, L. (2016) Geologia, petrologia e potencial para mineralizações magmáticas dos corpos máfico-ultramáficos da região de Canaã dos Carajás, Província Mineral de Carajás, Brasil. PhD Thesis, Universidade de Brasília.
83. Sillitoe, R. H. (2003) Iron oxide-copper-gold deposits: An Andean view. Mineralium Deposita, 38(7), 787–812. https://doi.org/10.1007/s00126-003-0379-7.
84. Silva, C. M. G. and Villas, R. N. (1998) The Águas Claras Cu-sulfide ± Au deposit, Carajás region, Pará, Brazil: geological setting, wall-rock alteration and mineralizing fluids. Revista Brasileira de Geociências, 28, 315–326.
85. Skirrow, R. G. (2022) Iron oxide copper-gold (IOCG) deposits—A review (part 1): Settings, mineralogy, ore geochemistry and classification. Ore Geology Reviews, 140, 104569. https://doi.org/10.1016/j.oregeorev.2021.104569.
86. Skirrow, R. G., Murr, J., Schofield, A., Huston, D. L., Van der Wielen, S., Czarnota, K., Coghlan, R., Highet, L. M., Connolly, D., Doublier, M. and Duan, J. (2019) Mapping iron oxide Cu-Au (IOCG) mineral potential in Australia using a knowledge-driven mineral systems-based approach. Ore Geology Reviews, 113, https://doi.org/10.1016/j.oregeorev.2019.103011.
87. Skirrow, R. G. and Walshe, J. L. (2002) Reduced and oxidized Au-Cu-Bi iron oxide deposits of the Tennant Creek Inlier, Australia: An integrated geologic and chemical model. Economic Geology, 97(6), https://doi.org/10.2113/gsecongeo.97.6.1167.
88. Souza, S. R. B., Macambira, M. J. B. and Sheller, T. (1996) Novos dados geocronológicos para os granitos deformados do Rio Itacaiúnas (Serra dos Carajás, PA); implicações estratigráficas. In: 5º Simpósio de Geologia da Amazônia, Belém, pp. 380–383.
89. Tallarico, F. H. B., Figueiredo, B. R., Groves, D. I., Kositcin, N., McNaughton, N. J., Fletcher, I. R. and Rego, J. L. (2005) Geology and SHRIMP U-Pb geochronology of the Igarapé Bahia deposit, Carajás copper-gold belt, Brazil: An Archean (2.57 Ga) example of Iron-Oxide Cu-Au-(U-REE) mineralization. Economic Geology, 100th Anni, 7–28.
90. Tallarico, F. H. B., McNaughton, N. J., Groves, D. I., Fletcher, I. R., Figueiredo, B. R., Carvalho, J. B., Rego, J. L. and Nunes, A. R. (2004) Geological and SHRIMP II U-Pb constraints on the age and origin of the Breves Cu-Au-(W-Bi-Sn) deposit, Carajás, Brazil. Mineralium Deposita, 39, 68–86.
91. Tallarico, F. H. B. (2003) O cinturão cupro-aurífero de Carajás, Brasil. Tese de Doutorado, Instituto de Geociências, UNICAMP, Campinas, 229.
92. Tazava, E. and Oliveira, C. G. (2000) The igarapé Bahia Au-Cu-(REE-U) deposit, Carajás Mineral Province, northern Brazil. In: Porter, T.M. (ed.) Hydrothermal Iron Oxide Copper-Gold & Related Deposits: A Global Perspective. Australian Mineral Foundation, Adelaide, pp. 203–212.

 doi:10.20944/preprints202508.1721.v1

93. Teixeira, A. S., Ferreira Filho, C. F., Giustina, M. E. S. D., Araujo, S. M. and Silva, H. H. A. B. (2015) Geology, petrology and geochronology of the Lago Grande layered complex: Evidence for a PGE-mineralized magmatic suite in the Carajás Mineral Province, Brazil. Journal of South American Earth Sciences, 64, 116–138.
94. Teixeira, W., Hamilton, M. A., Girardi, V. A. V., Faleiros, F. M. and Ernst, R. E. (2019) U-Pb baddeleyite ages of key dyke swarms in the Amazonian Craton (Carajás/Rio Maria and Rio Apa areas): Tectonic implications for events at 1880, 1110 Ma, 535 Ma and 200 Ma. Precambrian Research, 329, 138–155.
95. Torresi, I., Bortholoto, D. F. A., Xavier, R. P. and Monteiro, L. V. S. (2012) Hydrothermal alteration, fluid inclusions and stable isotope systematics of the Alvo 118 iron oxide-copper-gold deposit, Carajás Mineral Province (Brazil): Implications for ore genesis. Mineralium Deposita, 47, 299–323.
96. Trendall, A. F., Basei, M. A. S., De Laeter, J. R. and Nelson, D. R. (1998) SHRIMP U-Pb constraints on the age of the Carajás formation, Grão Pará Group, Amazon Craton. Journal of South American Earth Sciences, 11, 265–277.
97. Vale (2022) Formulário de Relatório Annual 20-F; Comissão de Valores Mobiliários dos Estados Unidos.
98. Vanko, D. A. and Bishop, F. C. (1982) Occurrence and origin of marialitic scapolite in the Humboldtt Lopolith, N.W. Nevada. Contributions to Mineralogy Petrology, 81, 277–289.
99. Vasquez, L. V., Rosa-Costa, L. R., Silva, C. G., Ricci, P. F., Barbosa, J. O., Klein, E. L., Lopes, E. S., Macambira, E. B., Chaves, C. L., Carvalho, J. M., Oliveira, J. G., Anjos, G. C. and Silva, H. R. (2008) Geologia e Recursos Minerais do Estado do Pará: Sistema de Informações Geográficas–SIG: Texto Explicativo dos Mapas Geológico e Tectônico e de Recursos Minerais do Estado do Pará. CPRM, Belém.
100. Vollgger, S. A., Cruden, A. R., Ailleres, L. and Cowan, E. J. (2015) Regional dome evolution and its control on ore-grade distribution: Insights from 3D implicit modelling of the Navachab gold deposit, Namibia. Ore Geology Reviews, 69, 268–284. https://doi.org/10.1016/j.oregeorev.2015.02.020.
101. Volp, K. M. (2005) The Estrela copper deposit, Carajás, Brazil. Geology and implications of a Proterozoic copper stockwork. In: Mao, J. and Bierlein, F.P. (eds.) Mineral Deposit Research: Meeting the Global Challenge. Springer, Berlin, pp. 1085–1088.
102. Williams, P. J., Barton, M. D., Johnson, D. A., Fontboté, L., de Haller, A., Mark, G., Oliver, N. H. S. and Marschik, R. (2005) Iron oxide copper-gold deposits: Geology, space-time distributions and possible modes of origin. Economic Geology, 100, 371–405.
103. Winter, C. J. (1994) Geology and base-metal mineralization associated with Archean iron-formation in the Pojuca Corpo Quatro Deposit, Carajás, Brazil. University of Southampton.
104. Wirth, K. R., Gibbs, A. K. and Olszewski, W. J. Jr. (1986) U-Pb ages of zircons from the Grão Pará Group and Serra dos Carajás granite, Pará, Brasil. Revista Brasileira de Geociências, 16, 195–200.
105. Xavier, R. P., Monteiro, L. V. S., Souza Filho, C. R., Torresi, I., Carvalho, E. R., Dreher, A. M., Wiedenbeck, M., Trumbull, R. B., Pestilho, A. L. S. and Moreto, C. P. N. (2010) The iron oxide copper–gold deposits of the Carajás Mineral Province, Brazil: an updated and critical review. In: Porter, T.M. (ed.) Hydrothermal Iron Oxide Copper-Gold & Related Deposits: A Global Perspective. Australian Miner. Fund, Adelaide, 3, 285–306.
106. Xavier, R. P., Monteiro, L. V. S., Moreto, C. P. N., Pestilho, A. L. S., Melo, G. H. C., Silva, M. A. D., Aires, B., Ribeiro, C. and Silva, F. H. F. (2012) The Iron Oxide Copper-Gold Systems of the Carajás Mineral Province, Brazil. In: Geology and Genesis of Major Copper Deposits and Districts of the World: A Tribute to Richard Sillitoe. Special publication of the Society of Economic Geologists.
107. Xavier, R. P., Moreto, C. P. N., Melo, G. H., Toledo, P., Hunger, R., Delinardo da Silva, M. A., Faustinoni, J., Lopes, A., Monteiro, L. V. S., Previato, M. and Jesus, S. S. (2017) Geology and metallogeny of Neoarchean and Paleoproterozoic copper systems of the Carajás Domain, Amazonian Craton, Brazil. In: Proceedings of the 14th Biennial SGA Meeting of the Society for Geology Applied to Mineral Deposits, Quebec.
108. Xavier, R. P., Monteiro, L. V. S., Moreto, C. P. N., Pestilho, A. L. S., Melo, G. H. C., Silva, M. A. D., Aires, B., Ribeiro, C. and Silva, F. H. F. 2012. The The Iron Oxide Copper-Gold Systems of the Carajás Mineral Province, Brazil. In: *Geology and Genesis of Major Copper Deposits and Districts of the World:* A Tribute to Richard Sillitoe. Special publication of the Society of Economic Geologists.

 doi:10.20944/preprints202508.1721.v1

109. Xavier, R. P., Moreto, C. P. N., Melo, G. H., Toledo, P., Hunger, R., Delinardo da Silva, M. A., Faustinoni, J., Lopes, A., Monteiro, L. V. S., Previato, M. and Jesus, S. S. 2017. Geology and metallogeny of Neoarchean and Paleoproterozoic copper systems of the Carajás Domain, Amazonian Craton, Brazil. In: *Proceedings of the 14th Biennial SGA Meeting of the Society for Geology Applied to Mineral Deposits*, Quebec, 899-902.
110. Zucchetti, M. 2007. *Rochas máficas do Grupo Grão Pará e sua relação com a mineralização de ferro dos depósitos N4 e N5, Carajás, PA*. Tese de Doutorado, UFMG, 165.